

# ADVANCED FE MODELING OF VEHICLE INTERIOR STRUCTURES TO ENHANCE THE PREDICTION FOR CRASH INDUCED INJURY RISK OF THE OCCUPANT

**Dae-Young Kim**

**Youngwan Kim**

**Ngoc-Trung Nguyen**

**Heon Young Kim**

Kangwon National University, Department of Mechanical and Biomedical Engineering

Korea, Republic of

**Hyung Yun Choi**

Hongik University, Department of Mechanical System Design Engineering

Korea, Republic of

Paper Number 13-0237

## ABSTRACT

Vehicle occupant's contact with the interior structure is the second collision at a crash event following the vehicle collision to foreign objects. Vehicle interior structure such as door trim, arm rest, instrumental panel, knee bolster, pillar trim, roof trim, and seat pad are made of various kinds of plastics and foams. The deformation and failure of these materials largely affect the kinematics and injury risks of the occupant. The major effort on virtual simulations of car crashworthiness has been focused on the precise modeling of load carrying primary metallic structures and crash dummies until now. The objective of this study is to advance the numerical modeling scheme of vehicle interior materials for their mechanical behaviors to simulate more realistic response of dummy kinematics and its associated injury risks. Plastic materials exhibit softening, dilatational, pressure dependent and anisotropic characteristics which should be considered during the modeling process as vehicle interior parts. In this paper, pros and cons of various material types in a crash code were comparatively analyzed. Both conventional modeling method for the steel material and Phenomenological model in LS-DYNA were respectively used to simulate plastic materials. Few coupon tests were conducted to identify basic material data for the Phenomenological model. Seating occupant is basically supported by the car seat and their interactions during the crash event affect the kinematics of occupant. The dynamic force-indentation characteristics of low density urethane foam at seat cushion and back are newly analyzed by measuring the exhalant airflow at impact test of pre-strained seat foams with trimming cover. A constitutive equation taking this airflow through the trimming

into account is under development and to be built in the existing material library of crash code.

## INTRODUCTION

The interior parts of vehicles are constructed of plastic and foam materials, due to their lightweight structure, ease of formability, and cost effectiveness in terms of manufacturing costs and fuel efficiency. However, these materials make it increasingly difficult to satisfy the crash performance and strength standards required by the enhanced safety regulations. Plastics are classified as crystalline or amorphous structures, according to the arrangement of cross-links that connect their molecular structure. Most vehicle interior parts consist of a combination of these two types of plastics, referred to as semi-crystalline plastics. The behavior of plastics can be described in terms of their softening characteristics, strength, and extension, as shown in (Figure 1).<sup>1-3)</sup>

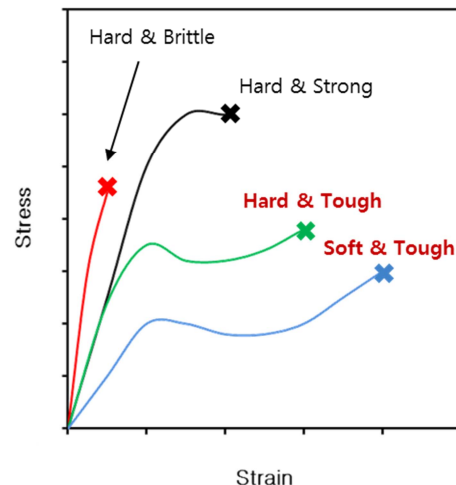


Figure 1. Classification of stress-strain curve of plastics

Constructing a material model for plastics, in terms of their structural analysis, is difficult due to their pressure dependency, dilatation, softening, and anisotropic properties. A von-Mises yield function and an isotropic hardening model have been used most often to represent the behavior of plastics in finite element analysis; however, this approach is not suitable for large deformation problems.<sup>4-6)</sup> So, the advanced or enhanced material model for plastics is needed and the test/calibration/correlation process are needed to improve the reliability.

In this paper, several material models, that are able to apply the plastic materials, are compared and analyzed. Also, SAMP-1 (Semi Analytical Model for Plastics) model is described in detail.<sup>7-9)</sup> Material test process and correlation process to obtain the parameter or data for SAMP-1 model are described. Finally, the SAMP-1 model is applied to FMH (free motion head-foam) impact analysis using the correlated parameters and data. Then the analysis results are compared with the analysis result of general material model.

In order to characterize the compression behavior (e.g., force-deformation relationship) of occupied (i.e., pre-strained) and trimmed (i.e., covered) low density PU foam in seat cushion and back, a dynamic compression machine using electromagnetic force is designed and built in this study. The design of the device enables to control the loading level and the amount of pre-strain of foam block. It is also feasible to measure exhalant air flow which significantly affects the reaction force at compression of PU foam, an highly porous material. The design of this electromagnetic machine and preliminary test result are introduced in this paper.

## MATERIAL MODELS

The deformation behavior of plastics can be explained by the molecular chain state. Yield appears after undergoing nonlinear elastic behavior, in which the molecular chains become unbound by application of an external force. After the occurrence of yield, softening, hardening, and rupture behaviors appear. LS-DYNA<sup>®</sup>, commercial FE code, provides several potential material models for plastics; these models are compared in (Table 1).

Although the Piecewise\_Linear\_Plasticity model (MAT24), generally applied to plastics, provides strain rates and fracture expressions, it cannot reflect the general characteristics of plastics.<sup>10)</sup> The Plasticity\_with\_damage model (MAT82) applies the von-Mises yield function and isotropic hardening model, similar to the Piecewise\_Linear\_Plasticity model, in addition to the Wilkins fracture model by

considering triaxial and asymmetric stress. The Polymer model (MAT168) is a physical model based on the mechanical behavior of the molecular structure.<sup>11)</sup> It has the advantage of being able to simulate both the elastic and plastic behaviors of plastics. However, this model does not consider strain rates, dilatation, or fracture characteristics, and requires an data of microscopic physical phenomena. The SAMP-1 model (MAT187) is based on a phenomenological model, and is much easier to apply than the Polymer model; it also has the advantage of being able to consider most characteristics of plastics.

**Table 1.**  
**Comparison of material models for plastics in LS-DYNA<sup>®</sup>**

Material model	24	82	89	101	106	112	141	168	187
Pressure dependent	N	N	N	Y	N	N	N	Y	Y
Volumetric response	N	N	N	N	N	N	N	N	Y
Failure	Y	Y	Y	Y	N	N	N	N	Y
Strain rate dependent	Y	Y	Y	Y	Y	Y	Y	N	Y
Temp. dependent	N	N	N	N	Y	N	N	Y	N
Softening	N	Y	N	N	N	N	N	Y	Y

The SAMP-1 model applies a yield model based on an isotropic C-1 smooth yield surface, expressed using a non-associated plastic flow rule. (Equation 1) shows the yield function, (Equation 2) describes the plastic potential, and (Equation 3) represents the relationship between the plastic Poisson's ratio,  $\nu_p$ , and the proportionality constant,  $\alpha$ . Because changes in the plastic Poisson's ratio affect the yield function, the SAMP-1 model can also consider characteristics of a plastic in terms of changes in its volume.

$$f = \sigma_{vm}^2 - A_0 - A_1 P - A_2 P^2 - A_3 P^3 \leq 0 \quad (1).$$

$$g = \sigma_{vm}^2 - \alpha P^2 \quad (2).$$

$$\nu_p = \frac{9 - 2\alpha}{18 + 2\alpha} \Rightarrow \alpha = \frac{9(1 - 2\nu_p)}{2(1 + \nu_p)} \quad (3).$$

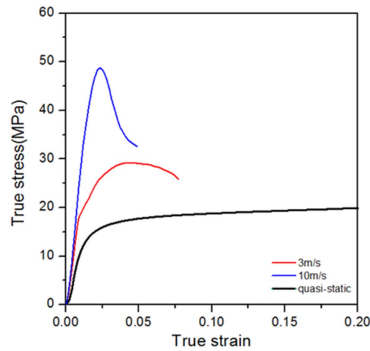
Where  $\sigma_{vm}$  gives the von-Mises stress,  $P$  is the pressure, and  $A_0$ ,  $A_1$ , and  $A_2$  correspond to the material constants. The material constants of the yield function, obtained from stress tests, are presented in (Equation 4) :

$$A_0 = 3\sigma_s^2; \quad A_1 = 9\sigma_s^2 \left( \frac{\sigma_c - \sigma_t}{\sigma_c \sigma_t} \right); \quad A_2 = 9 \left( \frac{\sigma_c \sigma_t - 3\sigma_s^2}{\sigma_c \sigma_t} \right) \quad (4).$$

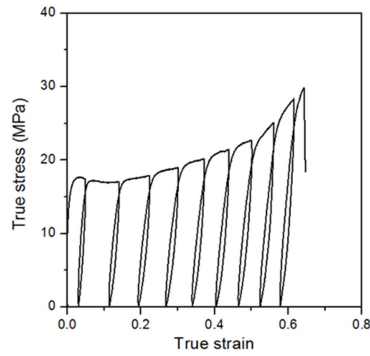
where  $\sigma_l$  is the uniaxial tensile stress,  $\sigma_c$  is the uniaxial compression stress, and  $\sigma_s$  is the shear stress. A simple damage model is used to express the softening characteristic:

$$D(\varepsilon_p) = 1 - \frac{E_d(\varepsilon_p)}{E} \quad (5).$$

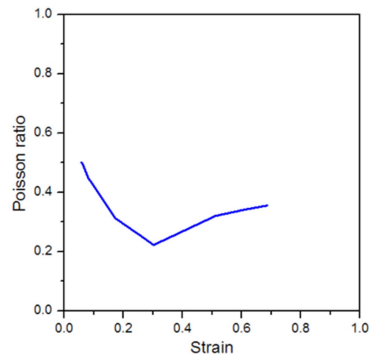
where  $D$  is the function for plastic strain,  $E$  is the elasticity coefficient, and  $E_d$  is the elasticity coefficient when a load is reapplied after removal of the previous load.



(a) Dynamic tension test



(b) Loading-Unloading test



(c) Measurement of Poisson's ratio

Figure 2. Results of material tests

## MATERIAL TESTS

### Plastics

Uniaxial tensile, shear, uniaxial compression, and biaxial tensile tests are required to apply the yield function of the SAMP-1 model. It is also necessary to measure changes in Poisson's ratio under uniaxial tensile conditions to evaluate the plastic characteristics as a function of volume change. Additionally, loading–unloading and dynamic tensile tests are required to study changes in the elasticity coefficients and strain-rate characteristics, respectively.

In this study, several tests were performed on PP-EPDM (polypropylene/ethylene-propylene-diene-monomer) materials. Specimens with a thickness of 3.2 mm were molded for the material tests. The uniaxial tensile tests made use of ASTM D 638 Type 1 specimens and an Instron 5882 universal testing machine (UTM).<sup>12)</sup> A cyclic loading tester, constructed specifically for this study, was used to test ASTM E 8 specimens for the uniaxial compression and loading–unloading tests.<sup>13)</sup> The dynamic tensile tests were performed on ASTM D 638 Type 4 specimens at speeds of 3 and 10  $\text{ms}^{-1}$ . To measure Poisson's ratio, 2 mm  $\times$  2 mm square lattices were printed on the surface of the specimens for the uniaxial tensile tests, and the displacement was traced by capturing the deformation conditions in each strain section. Based on the traced displacement, the strain ratio along the longitudinal and transverse directions was calculated to verify the data for Poisson's ratio. The test results are presented in (Figure 2).

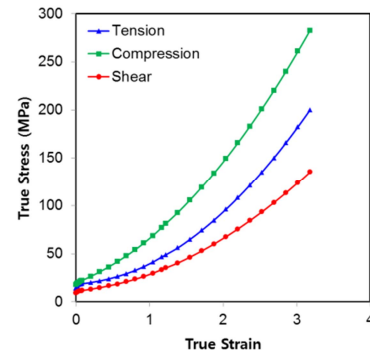


Figure 3. Plastic stress-strain curves

### Seat foam

Mostly due to the difficulties of controlling the amount of prestrain of foam block with the conventional drop weight type impact machine, a dynamic compression machine with utilizing electromagnetic force is substitutingly designed and built as shown in (Figure 4). Loading part of the device consists of two adjoined electromagnets and control unit. When control

unit is triggered to supply an electric current, both electromagnets are magnetized with same polarity and sudden repulsive force will be produced. Upper electromagnet is fixed at the frame of the barrel which has square cross section (100x100mm) but the lower electromagnet freely moves downward along the barrel and strikes the foam block. The peak striking force is modulated by the voltage level upto 100V and the prestrain of foam block can be easily adusted by positioning the initial electromagnets along the barrel upto 40% prestrain. The bottom plate supporting the foam block has 25 vent holes (5X5 with  $\Phi 6$ mm, D3574-08 ASTM<sup>14)</sup> through which the exhalant air can be gauged by flux sensors (ASF1430 Bidirectional Mass Flow, SENSIRION). Seat cover may be placed between foam block and perforated bottom plate to quantify the effect of air flow on the reaction force. Reaction force is measured by a loadcell (1kN, Testometric) positioned at the bottom of the supporting structure, i.e., barrel and perforated bottom plate.

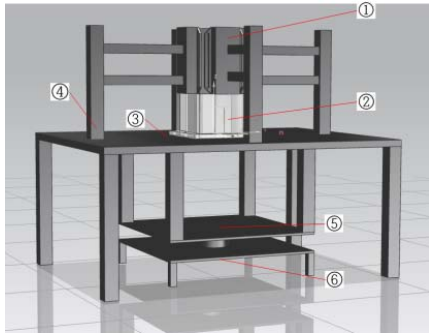


Figure 4. Dynamic compression device using electromagnets 1 Electromagnets, 2. Foam block, 3 Perforated bottom plate 4 Frame, 5 Upper load cell plate 6 Lower load cell plate

The preliminary test result is shown in (Figures 5-7). A foam block (Density: 48kg/m<sup>3</sup>, size: 100X100X100) and trimming pad cover for small sedan vehicle are employed. The reaction force profile measured at the load cell shows an initial sharp peak followed by a plateau and they both increase linearly with applied electric voltage level to the electromagnets (See Figure 5). The prestrain decrease the reaction force as shown in (Figure 6) but this possibly associates a misleading since the presented reaction force does not include initial preload developed by the given prestrain. As expected, the trimming pad placed between foam block and perforated bottom plate restricted exhalant air flow as shown in (Figure 7).

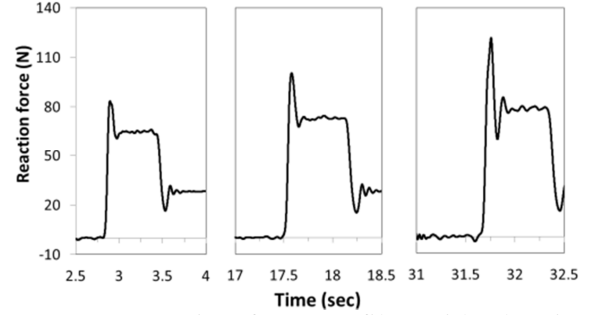


Figure 5. Reaction force profiles with electric voltage applied to the electromagnets, With no prestrain and trimming pad, left: 60V, middle: 80V, right: 100V

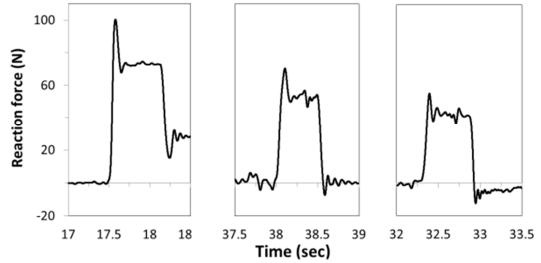


Figure 6. Reaction force profiles with prestrain, applied voltage to the electromagnets: 80V, left: 0% prestrain, middle: 20% prestrain, right: 40% prestrain.

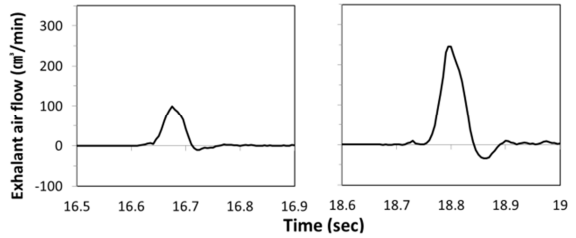


Figure 7. Reaction force profiles with and without trimming pad, applied voltage to the electromagnets: 50V, left: with pad, right: without pad

## CALIBRATION AND VERIFICATION

The various parameters from the material tests were calculated and supplied to the SAMP-1 model. The plastic regions after a yield point were also defined based on the results of the uniaxial tension and compression tests. The relationship between the shear stress and shear strain was determined based on the Drucker–Prager theory that defines the relationship between uniaxial tension, uniaxial compression, and shear stress:

$$\sigma_s = \frac{2\sigma_t\sigma_c}{\sqrt{3}(\sigma_t + \sigma_c)} \quad (6).$$

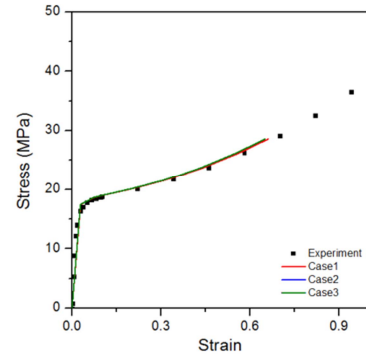
The stress–strain diagram of the uniaxial tension, uniaxial compression, and shear in the plastic region is presented in (Figure 3). However, it was necessary to transform the stresses because their scales varied according to changes in the observed damage and Poisson’s ratio.

FE analysis of a unit shell element model and ASTM D 638 tests for Type 1 specimens were used to verify the material model. As shown in (Table 2), an analysis was performed to determine the differences between a conventional material model and the SAMP-1 model.

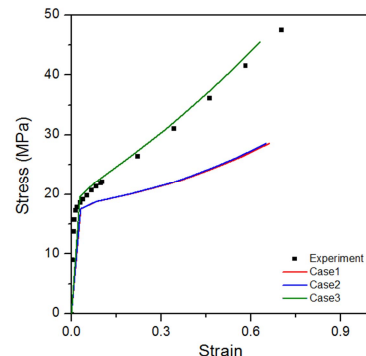
**Table 2.**  
**Analysis cases to compare the conventional model and SAMP-1 model**

Case	Model	Mode	Material model	S-S curve	Plastic Poisson’s ratio	Damage
Case 1	Unit shell element	Tension Compression Shear	Piecewise Linear Plasticity	Tension	0.5	N
Case 2	Unit shell element	Tension Compression Shear	SAMP-1	Tension	0.5	N
Case 3	Unit shell element	Tension Compression Shear	SAMP-1	Tension Compression Shear	0.5	N
Case 4	Specimen	Tension	Piecewise Linear Plasticity	Tension	0.5	N
Case 5	Specimen	Tension	SAMP-1	Tension Compression Shear	Curve	Curve

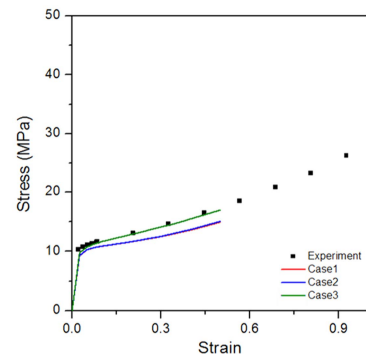
For cases 1, 2, and 3, the differences with respect to the yield functions of the Piecewise\_Linear\_Plasticity and SAMP-1 models were determined using the unit shell element model. The results are presented in (Figure 4). There was good agreement between the SAMP-1 model and the test results for uniaxial tension, uniaxial compression, and shear conditions. However, the Piecewise\_Linear\_Plasticity model results differed, indicating a constant yield stress for various pressures. Cases 4 and 5 compared the Piecewise\_Linear\_Plasticity and SAMP-1 models using ASTM D 638 Type 1 specimens. SAMP-1 was defined with respect to the observed damage and Poisson’s ratio. The results of these cases are presented in (Figure 8) and (Figure 9). The Piecewise\_Linear\_Plasticity model indicated large localized deformations, while the SAMP-1 model was in good agreement with the test results. The SAMP-1 model showed transverse changes in the surrounding elements after necking, similar to the tests, because dilatation was considered in this model.



(a) Tension mode



(b) Compression mode



(c) Shear mode

Figure 8. Analysis results using unit shell model

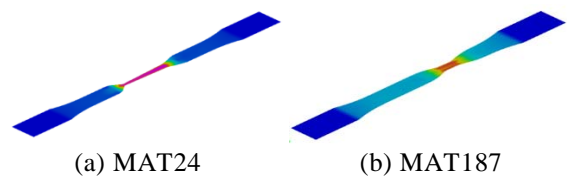


Figure 9. Comparison of deformed shapes

## APPLICATION

To apply the SAMP-1 model to the interior materials in vehicles, an impact analysis for the pillar inner trim was performed based on FMVSS201U for the impact of interior materials established by the

National Highway Traffic Safety Administration (NHTSA).<sup>15</sup> FMVSS201U regulates the value of the head injury criterion (HIC). HIC(d), the equivalent value of the head injury criterion, did not exceed 1000 free-motion head (FMH) strikes against 16 impact points on the upper interior parts of the vehicle for a vehicle traveling at a speed of 15 mph. The FMH model, provided by Livermore Software Technology Corporation (LSTC), was used for the impact analysis and to determine the boundary conditions required to introduce bending and collapse deformations, as shown in Figure 11. The strain rates obtained from the PIECEWISE\_LINEAR\_PLASTICITY and SAMP-1 models were compared. Also, the true stress–true strain curve, measured from the dynamic tensile tests, was fitted using the G’Sell–Jonas model presented in (Equation 7).<sup>16</sup> The G’Sell–Jonas model includes the material behavior characteristics of viscoelasticity, viscoplasticity, and temperature,

$$\sigma(\dot{\epsilon}, \epsilon, T) = K(\dot{\epsilon})^m e^{h\epsilon^2} (1 - e^{-w\epsilon}) e^{\frac{a}{T}} \quad (7).$$

where  $K$ ,  $a$ ,  $w$ ,  $h$ , and  $m$  are the material constants, and  $T$  is the absolute temperature.

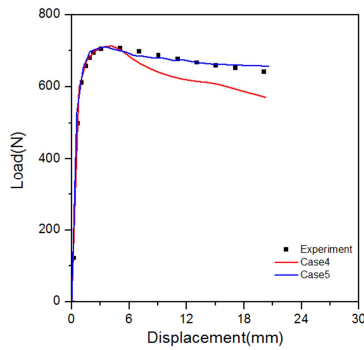


Figure 10. Comparison of L-D curve

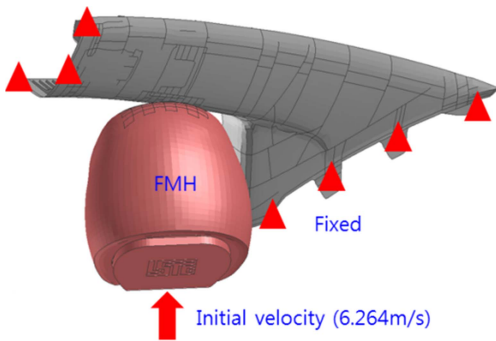


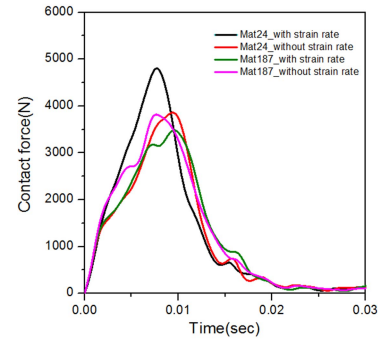
Figure 11. Boundary condition for FMH impact analysis

From the analysis results, it was possible to obtain the contact pressure and acceleration diagram, as shown in (Figure 12). HIC (d) is calculated using the acceleration diagram; the HIC value is given by (Equation 8), in which  $a(t)$  is the three-axis composition acceleration of the center of mass in the FMH model, and  $t_1$  and  $t_2$  represent random times of presenting the maximum injury below 36 ms in the impact event. HIC(d) can be represented by (Equation 9) to determine the correlation to the head injury level in a practical impact test using a test dummy.<sup>17-19)</sup>

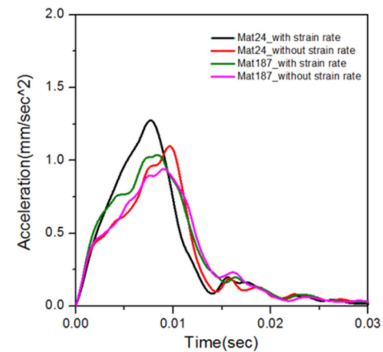
$$HIC = \max \left[ \left( \frac{1}{t_2 - t_1} \int_{t_1}^{t_2} a(t) dt \right)^{2.5} (t_2 - t_1) \right] \quad (8).$$

$$HIC(d) = 166.4 + (0.75446 \times HIC) \quad (9).$$

The results from the PIECEWISE\_LINEAR\_PLASTICITY model, with and without consideration of the strain rate, were 12.67 and 18.45, respectively. This varied significantly from the results provided using the SAMP-1 model, which were 11.71 and 14.97 with and without strain-rate consideration, respectively.



(a) contact force curves



(b) Acceleration curves

Figure 12. Comparison of results for FMH impact analysis

## CONCLUSION

Material models that could be applied to the LS-DYNA simulation software were compared to implement material modeling for plastic materials. Several material tests were performed using the SAMP-1 model. A method for obtaining the parameters and material data was proposed based on these tests. The proposed models were verified using a unit model and a specimen model of a shell element. Differences between the proposed material model and the conventional material model were analyzed. There was good agreement between the SAMP-1 model and the test results for material tests. The large differences in the results for each model could be explained based on whether or not a model considered the strain rates determined from FMH impact analysis for the pillar inner trim of vehicles. In order to effectively realize the prestrain of seat foam which represents an occupied condition into the dynamic compression test, electromagnets are introduced to substitute the conventional test device such as drop weight. From the preliminary test result even though in a limited range, the device verified its good repeatability and efficiency for characterizing the compression behavior of seat foam with various loading and prestrain conditions. Utilizing flux sensors, it becomes also feasible to gauge the exhalant air and thus quantify the effect of trimming pad cover which interferes with the air flow. This new and additional characterization in deformation behavior of seat foam will be incorporated into crash codes as a more advanced material card.

## REFERENCES

- [1] Andrzej Pawlak and Andrzej Galeski. 2005. "Plastic Deformation of Crystalline Polymers." American Chemical Society, Vol. 38, No. 23, 9688-9697
- [2] A. Blaga. 1973. "Properties and Behaviour of Plastics." NRC
- [3] G'Sell, C. 1986. "Plastic deformation of glassy polymers: constitutive equations and macromolecular mechanisms." *Ocfor*, 1943-1982
- [4] Arild Holm Clausen, Mario Polanco-Loria, Torodd Berstad and Odd Sture Hopperstad. 2011. "A CONSTITUTIVE MODEL FOR THERMOPLASTICS WITH SOME APPLICATIONS." 8th European LS-DYNA Users Conference
- [5] M. Avalle, M. Peroni and A. Scattina. 2010. "Mechanical models of the behaviour of plastic materials: influence of time and temperature." Latin American Journal of Solids and Structures, 41-61
- [6] M.C. Boyce, S. Socrate, P.G. Llana. 2000. "Constitutive model for the finite deformation stress-strain behavior of poly (ethylene terephthalate) above the glass transition." *Polymer*, Vol. 41, No. 6, March: 2183-2201
- [7] LIVERMORE SOFTWARE TECHNOLOGY CORPORATION (LSTC). 2007. "LS-DYNA KEYWORD USER'S MANUAL VOLUME I"
- [8] S. Kolling, A. Haufe, M. Feucht & P.A. Du Bois. 2005. "SAMP-1: A Semi-Analytical Model for the Simulation of Polymers." LS-DYNA Anwender forum
- [9] Kunio TAKEKOSHO and Kazukuni NIWA. 2012. "Validation and Material Modeling of Polymers by Employing MAT\_SAMP-1." 12th International LS-DYNA Users Conference
- [10] M. Vogler, S. Kolling, A. Haufe. 2007. "A Constitutive Model for Plastics with Piecewise Linear Yield surface and Damage." LS-DYNA Anwender forum
- [11] M. Polanco-Loria<sup>1</sup>, H. Daiyan and F. Grytten. 2012. "Material parameters identification: An inverse modeling methodology applicable for thermoplastic materials." *Polymer Engineering & science*, Vol. 52, No. 2, February: 438-448
- [12] ASTM D638-10. 2010. "Standard Test Method for Tensile Properties of Plastics" ASTM International, Vol. 08.01
- [13] ASTM E8-11. 2011. "Standard Test Method for Tension Testing of Metallic Materials." ASTM International, Vol. 03.01
- [14] ASTM D3574-08 Standard Test Methods for Flexible Cellular Materials - Slab, Bonded, and Molded Urethane Foams
- [15] Hyoung Gon Kim, Shinill Kang. 2001. "Optimum Design of A-Pillar Trim for Occupant Protection." *KSAE*, Vol. 9, No. 2, 99-106
- [16] Marcus Schoßig, Christian Bierogel, Wolfgang Grellmann, Thomas Mecklenburg. 2008. "Mechanical behavior of glass-fiber reinforced thermoplastic materials under high strain rates." *Polymer Testing*, Vol. 27, July: 893-900
- [17] FMVSS 201U: Occupant Protection in Interior Impact Upper Interior Head Impact Protection. 1998. Federal Motor Vehicle Safety Standard, National Highway Traffic Safety Administration, U.S. Department of Transportation
- [18] Younghan Youn, Youngki Kim, Hyeongyo Park, Heesang An. 2005. "Analytical Studies on the Pillar Trim Impact Test Using FMH." Autumn conference of proceedings of the KSAE, 1491-1495
- [19] Bharatendra Rai, Nanua Singh, Mustafa Ahmed. 2004. "Robust design of an interior hard trim to improve occupant safety in a vehicle

crash.” Reliability Engineering and System  
Safety, Vol. 89, 296-304